Available online at www.sciencedirect.com
ScienceDirect
Journal of Power Sources 178 (2008) 490–496
JOURNAL OF POWER SOURCES
www.elsevier.com/locate/jpowsour

High voltage, asymmetric EDLCs based on xerogel carbon and hydrophobic IL electrolytes

M. Lazzari, F. Soavi, M. Mastragostino *

University of Bologna, Department of Metal Science, Electrochemistry and Chemical Techniques, Via San Donato 15, 40127 Bologna, Italy

Received 23 October 2007; received in revised form 7 December 2007; accepted 8 December 2007
Available online 1 February 2008

Abstract

The preparation procedure, morphology and the surface chemistry of xerogel carbons, which exhibited up to 120 F g^{-1} in ionic liquid (IL) at 60 °C, are reported. Performance results of double-layer supercapacitors (EDLCs) featuring an asymmetric configuration with mesoporous xerogel carbon electrodes and hydrophobic ionic liquid electrolyte operating at 60 °C are also shown. The investigated ILs are 1-ethyl-3-methyl-imidazolium-bis(trifluoromethanesulfonyl)imide (EMITFSI) and *N*-butyl-*N*-methylpyrrolidinium-bis(trifluoromethanesulfonyl)imide (PYR_{14}TFSI). While the PYR_{14}TFSI features lower conductivity and determines slightly lower xerogel carbon capacitive response than EMITFSI, it enables a wider potential excursion for the negative electrode charging process. This is beneficial for high maximum cell voltages (V_{max}) and, thus, for both the specific energy and power of asymmetric EDLCs. The asymmetric configuration we developed, with higher carbon loading at the positive electrode than that at the negative, makes it possible to tune the potential excursion of each electrode so that the EDLCs with EMITFSI and PYR_{14}TFSI attain the safe V_{max} of 3.4 V and 3.7 V, respectively, and high specific energy of ca. 30 Wh kg^{-1} between V_{max} and $0.5V_{max}$ over several thousand cycles.
© 2007 Elsevier B.V. All rights reserved.

Keywords: Supercapacitor; Ionic liquid; Xerogel carbon; Asymmetric EDLC; Capacitance

1. Introduction

Much effort is being focused on the development, and operating temperature, of high specific energy, E_{max}, double-layer carbon supercapacitors (EDLCs). Indeed, one field of EDLC application is transportation requiring high-efficiency electrochemical energy storage/conversion systems, even above RT. Given that E_{max} depends on supercapacitor specific capacitance (C_{EDLC}) and maximum cell voltage (V_{max}) as in the following equation, when evaluated between V_{max} and $0.5V_{max}$:

$$E_{max} = \frac{3}{8} C_{EDLC} V_{max}^2, \quad (1)$$

the pursued strategies are basically devoted to the development of high specific double-layer capacitance carbons and of safe, non-aqueous electrolytes with a wide electrochemical stability window (ESW) and high ionic conductivity for high specific power [1–4].

Ionic liquids (ILs) of wide ESW and good conductivity above RT are under investigation for high-voltage supercapacitors operating at $T > RT$, where they work as "solvent-free" electrolytes. Note that the properties of these ILs like polarizability also directly affect the electrode/electrolyte interface and, thus, supercapacitor capacitance. For high specific capacitance in ILs the carbon electrodes should display a high surface area that is easily accessible to the IL ions involved in the double-layer formation. This can be achieved by optimization of carbon surface chemistry and morphology. Given that IL purity is of paramount importance for long supercapacitor cycle-life and a high level of purity is more readily attainable for hydrophobic ILs, hydrophilic moieties that may repel IL ions should be absent from the carbon surface. IL ions typically have a size in the order of 1 nm so that for fast double-layer charging processes the carbon surface should mainly be made up of large micropores and mesopores. Xerogel carbons that are characterized by hydrophobic surfaces and a mesopore surface area tunable by synthesis conditions thus look like good electrode materials for IL-based EDLCs. Their capacitance responses at 60 °C in such hydrophobic ILs as 1-ethyl-3-methyl-imidazolium-bis(trifluoromethanesulfonyl)imide (EMITFSI) and *N*-butyl-*N*-me-

* Corresponding author. Tel.: +39 051 2099798; fax: +39 051 2099365.
E-mail address: marina.mastragostino@unibo.it (M. Mastragostino).

0378-7753/$ – see front matter © 2007 Elsevier B.V. All rights reserved.
doi:10.1016/j.jpowsour.2007.12.029

thylpyrrolidinium-bis(trifluoromethanesulfonyl)imide (PYR_{14}TFSI) has been estimated at ca. 0.2 F m^{-2} of mesoporous surface area [5–10].

Since the mid-point of the ESW of the ILs is not usually found at the potentials of the discharged carbon electrodes, only by assembling asymmetric EDLC configurations featuring different loading of the same carbon at the two electrodes is it possible to charge each electrode up to the limit potential defined by IL stability and, hence, to reach maximum cell voltages significantly higher than those achievable with symmetric EDLC configurations [11].

We thus set out to develop xerogel carbons with a mesopore surface area higher than 500 m^2 g^{-1}, so as to provide at least 100 F g^{-1} at 60 °C in the hydrophobic ILs EMITFSI and PYR_{14}TFSI, and report the results. We also include the cycling performance of asymmetric EDLCs with a xerogel carbon with a mesopore area of 600 m^2 g^{-1} operating in EMITFSI and in PYR_{14}TFSI at 60 °C at high voltages over several thousands cycles. The viability of the asymmetric EDLC configuration was investigated with both ILs since the former is attractive for its higher ionic conductivity and the latter for its wider ESW.

2. Experimental

The xerogel carbons X1p, X2p and X3p were prepared by polycondensation of resorcinol and formaldehyde with Na_2CO_3 as gelation catalyst in different molar ratios, followed by solvent exchange, RT drying and pyrolysis at 850–1050 °C in Ar as in Ref. [10]; the pyrolysed carbons were then soft milled. The xerogel carbon powders were also treated in CO_2 (200 cm^3 min^{-1}) at 850–1050 °C over different time intervals (t_{CO_2}) and kept 1 h in Ar (200 cm^3 min^{-1}) at the same temperature in order to remove any surface moieties formed during activation; heating (10 °C min^{-1}) and cooling were carried out in Ar and the treated carbons are labelled X1a, X2a, X3a.

Nitrogen adsorption porosimetry measurements were carried out at 77 K with an ASAP 2020 system (Micromeritics); the carbon powders were dried for at least 2 h at 120 °C before testing. The N_2 adsorption isotherms were analyzed by density functional theory (DFT) and the specific surface area related to pores wider than 1.5 nm ($S_{>1.5nm}$) was evaluated from DFT mesoporous volume by assuming a cylindrical pore geometry. FTIR spectra in reflectance mode (FTIR-ATR) were collected by a PerkinElmer Spectrometer Spectrum ONE (FTIR-ATR) with 40 scans and 4 cm^{-1} resolution.

The carbon electrodes (ca. 0.6 cm^2 geometric area; 6–13 mg cm^{-2} carbon loading) were prepared by mixing 95% (w/w) carbon and 5% (w/w) polytetrafluoroethylene binder (DuPont) to yield a paste which was then laminated on carbon coated aluminum grids (Lamart Corp.).

The PYR_{14}TFSI (Solvent Innovation, 98%) and EMITFSI (Solvent Innovation, 99%) ILs were dried over night at 80 °C under dynamic vacuum (Büchi Glass Oven B-580) and displayed ca. 30 ppm of water as checked by Karl Fisher titration (684 KF Coulometer Metrohm).

We used Swagelok-type, "three electrodes" cells for single electrode and supercapacitor tests. A silver disk was used as quasi-reference electrode for the cyclic voltammetries and to check electrode potentials during supercapacitor galvanostatic cycling. The silver disk potential, measured in conventional cells prior to the electrochemical tests by adding the highly reversible redox couple ferrocene/ferrocinium (Fc/Fc^+) to the medium, was E_{Ag} (V) = (E_{Fc/Fc^+} + 0.200 ± 0.010); hereinafter the electrode potentials are given versus Fc/Fc^+ for comparison with literature. The cells were assembled in dry box (MBraun Labmaster 130, H_2O and O_2 <1 ppm) by facing two carbon composite electrodes and using a fiber glass separator (Durieux, 200 μm thick when pressed); for single-electrode studies, double-layer carbon counter-electrodes with charge storage capability significantly higher than that of the working electrodes were used so as not to limit the capacitive response of the working electrode. The cells were kept at a controlled temperature of 60 ± 2 °C using a Thermoblock (FALC). The electrochemical tests were performed with a PerkinElmer VMP multichannel potentiostat/galvanostat and a Solartron SI 1255 frequency-response analyzer coupled to a 273A PAR potentiostat/galvanostat. Impedance spectra were recorded with 5 mV ac perturbation in the frequency range of 50 kHz to 10 mHz.

3. Results and discussion

Table 1 summarizes the synthesis conditions and the porosity data of the xerogel carbons evaluated from the N_2 adsorption isotherms reported in Fig. 1. Fig. 2 shows the pore-size distri-

Table 1
Synthesis conditions in terms of resorcinol to gelation catalyst (*R/C*) and of water to resorcinol, formaldehyde and gelation catalyst (*D*) molar ratios, pH of the gelation bath and CO_2 activation time (t_{CO_2}); total pore volume (V_{tot}), percentage of pore volume ($V_{>1.5nm}$) and specific surface area ($S_{>1.5nm}$) related to pores wider than 1.5 nm, mean mesopore size (d_p) of the pristine (X1p, X2p, X3p) and CO_2/Ar treated (X1a, X2a, X3a) carbon powders from the DFT analysis of the corresponding N_2 adsorption isotherms at 77 K

Carbon	Synthesis conditions				Porosity			
	R/C	*D*	pH	t_{CO_2} (h)	V_{tot} (cm^3 g^{-1})	$V_{>1.5nm}$ (%)	$S_{>1.5nm}$ (m^2 g^{-1})	d_p (nm)
X1p	200	2.5	6.40	–	0.28	64	185	5
X2p	300	5.7	6.50	–	0.96	83	315	14
X3p	400	4	6.53	–	1.03	87	310	15
X1a	200	2.5	6.40	2.5	0.82	63	375	6
X2a	300	5.7	6.50	4.0	1.29	77	410	14
X3a	400	4	6.53	5.5	1.73	77	600	15

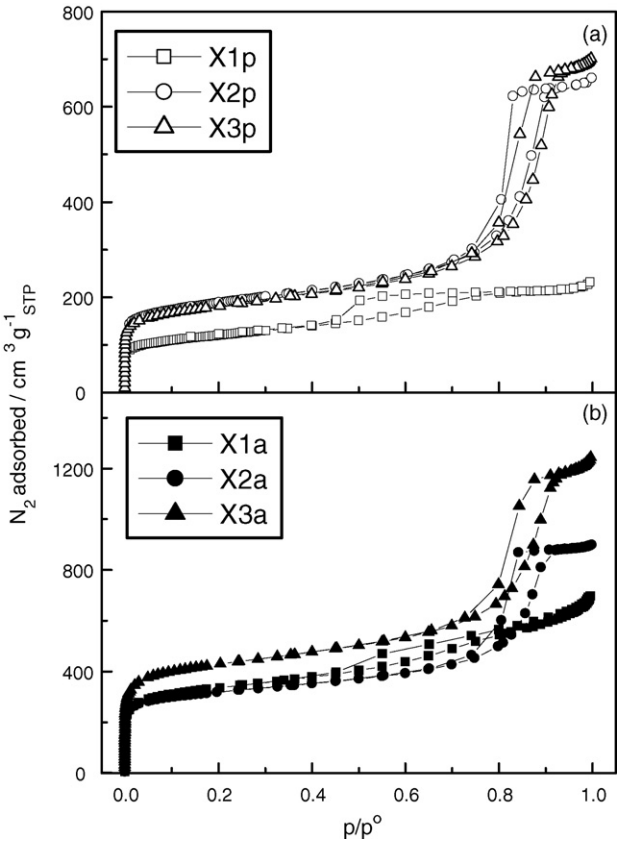

Fig. 1. N_2 adsorption/desorption isotherms at 77 K of (a) pristine and (b) treated xerogel carbons.

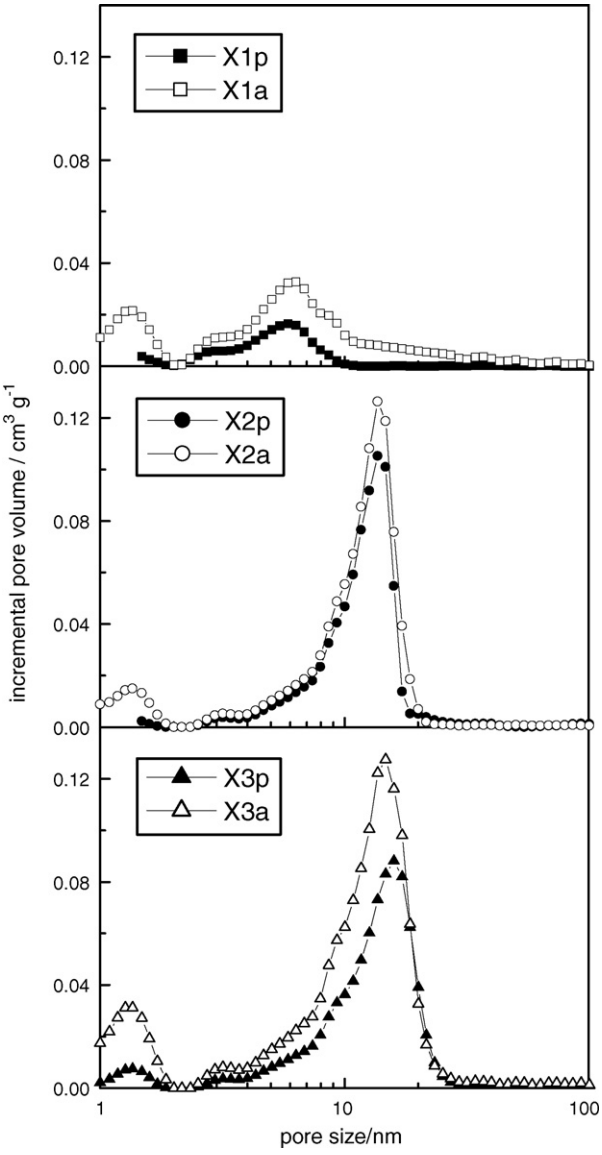

Fig. 2. DFT incremental pore volume vs. pore size of the pristine X1p, X2p and X3p and treated X1a, X2a and X3a xerogel carbons.

bution in incremental pore volume for the different carbons and shows that the pores in all the carbons are sufficiently wide to be filled with the ILs. Xerogel carbon X1p exhibits the lowest porosity, with 5 nm pores accounting for 64%. The data in Table 1 indicate that by increasing the *R*/*C* and *D* parameters from 200 to ≥300 and from 2.5 to ≥4, respectively, the total pore volume (V_{tot}) of the pristine carbon reaches 1 $cm^3\ g^{-1}$ while maintaining a high percentage of volume from pores >1.5 nm ($V_{>1.5nm}$). The increase of *R*/*C* and *D* also widens the pores to ca. 15 nm so that the gain in surface area is lower than expected. Indeed, the specific surface area related to pores wider than 1.5 nm ($S_{>1.5nm}$), i.e. to the mesopores and large micropores involved in the double-layer charging process, only doubles, roughly, with the X2p and X3p carbons. We thus treated the X1p, X2p and X3p xerogel carbons using a two-step procedure: CO_2 activation at 850–1050 °C for the increase of the surface area, followed by heat-treatment in Ar at the same temperature for the removal of any hydrophilic, oxygen-containing surface moieties formed along the previous activation step; the corresponding treated xerogel carbons are X1a, X2a and X3a. The data in Table 1 and Fig. 2 show that treatments significantly increased total pore volume (micropores included) of the carbons without modifying their mesopore size distribution, a fact that might be explained by the carbon pores' lengthening while retaining the same width. While an activation time of 2.5 h provided an $S_{>1.5nm}$ double that of X1p for carbon X1a, longer treatments of 4 and 5.5 h were necessary for X2a and X3a to yield $S_{>1.5nm}$ of 410 and 600 $m^2\ g^{-1}$, respectively. The FTIR-ATR spectrum of X3a in Fig. 3 indicates that the two-step activation procedure does not yield carboxyl-based acid surface moieties, which are the main cause of the hydrophilic behaviour of carbons and which should give strong absorption bands at ca. 1600 cm^{-1}; the weak and broad band in the region can rather be ascribed to aromatic C=C vibrations. Indeed, the main absorptions in the spectrum in Fig. 3, at 2160, 2030 and 1975 cm^{-1} and in the 900–1300 cm^{-1} region, are related to the C=O stretching in chetenes and cyclic anhydrides and to the C–O stretching in ethers, phenols and cyclic anhydrides, respectively, i.e. to basic or weak acidic moieties [12–14].

The surface features of the treated xerogel carbons enable a high IL uptake and, hence, high capacitive responses as shown by the data in Table 2, which reports the specific capacitances

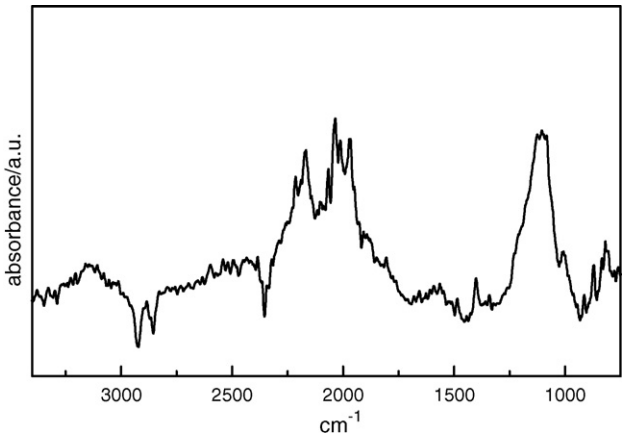

Fig. 3. FTIR-ATR spectrum of the X3a treated xerogel carbon.

Table 2
Specific capacitance (C) of the treated xerogel carbons in EMITFSI and $PYR_{14}TFSI$ at 60 °C in different potential ranges (ΔV, potentials given vs. Fc/Fc^+) as evaluated from the voltammetric discharges at 20 mV s^{-1} by the slope of the integral over time of the current vs. electrode potential

Carbon	EMITFSI		$PYR_{14}TFSI$	
	ΔV (V)	C (F g^{-1})	ΔV (V)	C (F g^{-1})
X1a	−2.1/−0.1	90 ± 6	−2.1/−0.1	75 ± 8
X2a	−2.1/−0.1	106 ± 6	−2.6/−0.1	87 ± 13
X3a	−2.1/−0.1	125 ± 6	−2.6/−0.1	108 ± 15
	−0.1/1.3	128 ± 12	−0.1/1.4	120 ± 20

(C) of the X1a, X2a and X3a carbons delivered in the two ILs at 60 °C in different electrode potential domains. When the same IL is considered, the specific capacitance increases in the order of X1a < X2a < X3a, i.e. with the carbon's $S_{>1.5nm}$. X3a, the carbon with the highest $S_{>1.5nm}$ of 600 m^2 g^{-1}, exceeds 100 F g^{-1} in both ILs, reaching 125 F g^{-1} in EMITFSI; notably these values were reached at high specific currents, higher than 2 mA mg^{-1}, as shown by the CVs reported in Fig. 4. For each negatively charged carbon, the specific capacitance is ca. 20% higher in EMITFSI than in $PYR_{14}TFSI$, as expected on the basis of the different nature of the ILs counterions involved in the double-layer, which also affect the potential limits for the charge/discharges at high coulombic efficiency [9]. While in EMITFSI the negative electrode cannot be polarized below −2.1 V versus Fc/Fc^+, mainly because of the presence of the labile acid proton of the imidazolium ring, in $PYR_{14}TFSI$ it is possible to reach −2.6 V versus Fc/Fc^+. Table 2 also reports the specific capacitance in the positive domain of the best-performing X3a carbon. In both the ILs the potential excursions of the positive electrodes are limited by the $TFSI^-$ anion stability and cannot exceed 1.6 V versus Fc/Fc^+ (higher than the value reported in Table 2). Given that the typical potential of the discharged electrodes is ca. −0.1 V versus Fc/Fc^+, the maximum potential excursion for the positive electrode can be 1.7 V, narrower than that achievable with the negative electrode, which is ca. 2.0 V in EMITFSI and 2.5 V in $PYR_{14}TFSI$. Thus, in a conventional symmetric configuration of EDLC, where the two electrodes have the same carbon loading and almost the same specific capacitance, i.e. the same charge storage capability, the maximum potential excursion for the negative electrode would be limited by that of the positive, as shown by the following equation:

$$\Delta V_- = \frac{C_+ w_+ \Delta V_+}{C_- w_-}, \quad (2)$$

where C_+, w_+, ΔV_+ and C_-, w_-, ΔV_- are the specific capacitance, carbon loading and maximum potential excursion of the positive and negative electrode, respectively. In other words, symmetric EDLCs can safely operate below 3.4 V with both the ILs and, particularly in the case of $PYR_{14}TFSI$, do not take full advantage of the electrolyte's wide ESW. Asymmetric configurations with positive-to-negative electrode mass loading ratios, $R_{+/-}$, higher than 1 would make it possible to widen the negative electrode potential excursions up to the values allowed by the ESW of the ILs while keeping the same ΔV_+, so that up to 4.2 V could be achieved with $PYR_{14}TFSI$-based EDLCs.

We then assembled asymmetric EDLCs with both ILs and the best performing X3a xerogel carbon using $R_{+/-} > 1$ as reported in Table 3, which also shows the total composite electrode mass loadings of the supercapacitors (w_{EDLC}, positive and negative electrodes together). The EMITFSI and $PYR_{14}TFSI$-based EDLCs were tested at 60 °C with $V_{max} \leq 3.4$ V and ≤3.7 V, respectively, in order to keep the cells sufficiently far from the envisioned potential limits in view of long-term cycling tests and with operating potentials still significantly higher than those feasible with commercial supercapacitors. Fig. 5 shows the galvanostatic profiles of the charge/discharge cycles at 10 mA cm^{-2} with $V_{max} = 3.3$ V and 3.7 V of the X3a/EMITFSI/X3a and X3a/$PYR_{14}TFSI$/X3a asymmetric EDLCs and of the corresponding electrodes collected after 5600 and 15,300 cycles, respectively, at 20 mA cm^{-2}; the dashed lines indicate the maximum electrode potential excursions permitted by the ILs. While in Fig. 5a the electrode potential profiles indicate that

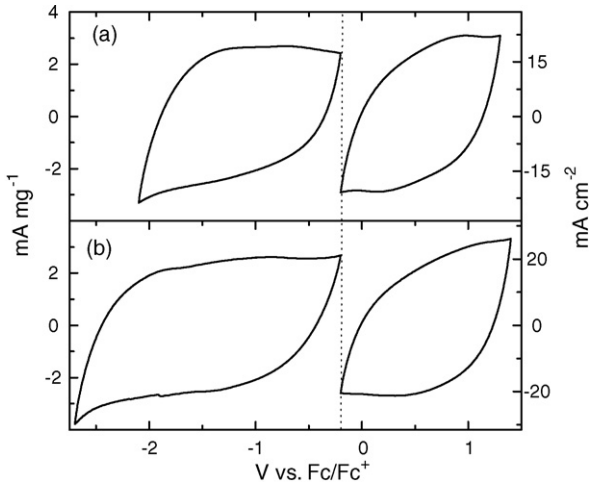

Fig. 4. CVs at 20 mV s^{-1} and 60 °C of X3a carbon electrodes in (a) EMITFSI and (b) $PYR_{14}TFSI$.

Table 3
Values of positive to negative mass loading ratio ($R_{+/-}$) and of total composite electrode mass loading (w_{EDLC}, positive and negative electrodes together) of the asymmetric EDLCs with EMITFSI and $PYR_{14}TFSI$ electrolytes, and maximum cell voltage V_{max}, supercapacitor specific capacitance (C_{EDLC}, on the basis of w_{EDLC}), maximum specific energy (E_{max}), equivalent series resistance (ESR, by the ohmic drop after 0.1 s from the beginning of discharge) and maximum specific power (P_{max}) at the 12,000th and 11,000th galvanostatic cycle, respectively, at 20 mA cm^{-2} and 60 °C

IL	$R_{+/-}$	w_{EDLC} (mg cm^{-2})	V_{max} (V)	C_{EDLC} (F g^{-1})	E_{max} (Wh kg^{-1})	ESR (Ω cm^2)	P_{max} (kW kg^{-1})
EMITFSI	1.4	20.4	3.4	26	31	15	9.5
$PYR_{14}TFSI$	1.6	15.0	3.7	21	30	20	11.4

in the X3a/EMITFSI/X3a EDLC electrode mass balance is almost optimized, the profiles in Fig. 5b indicate that in the X3a/$PYR_{14}TFSI$/X3a the $R_{+/-}$ parameter could be increased slightly in order to attain higher V_{max} by a wider sweep of the negative electrode potential ΔV_- while keeping the same ΔV_+.

Both supercapacitors were tested over several thousand cycles at 20 mA cm^{-2} and 60 °C; Table 3 reports the maximum cell voltage V_{max}, the specific capacitance (C_{EDLC}) and the maximum specific energy (E_{max}) of the supercapacitors after more than 10,000 galvanostatic cycles. At the 12,000th cycle, the X3a/EMITFSI/X3a EDLC delivers 26 F g^{-1} of total composite electrode materials and a maximum specific energy between 3.4 V and 1.7 V of 31 Wh kg^{-1}. At the 11,000th cycle, the supercapacitor with $PYR_{14}TFSI$ delivers a slightly lower capacitance of 21 F g^{-1} (as expected on the basis of single electrode tests) and the corresponding energy delivered between 3.7 V and 1.85 V is of 30 Wh kg^{-1}, a value which can be increased if a better electrode balancing that enables to reach at least 4.0 V is used. These results are very interesting not only because the E_{max} exceeds by 30% that delivered by symmetric EDLC with $PYR_{14}TFSI$ and commercial activated carbons [8], thus demonstrating the potency of the asymmetric configuration and of xerogel carbons, but mainly because they were quite stable over several thousand cycles as shown in Fig. 6. This figure reports the trend of C_{EDLC} over cycling at 60 °C and 20 mA cm^{-2} for the two EDLCs carried out with V_{max} up to 3.4 V in the case of X3a/EMITFSI/X3a and with V_{max} up to 3.7 V in the case of X3a/$PYR_{14}TFSI$/X3a (800 cycles were also performed with V_{max} = 3.9 V).

Table 3 also shows the maximum specific power P_{max} of the two EDLCs at 60 °C calculated by $P_{max} = V_{max}^2/(4ESR\, w_{EDLC})$, where ESR is the equivalent series resistance evaluated by the ohmic drop after 0.1 s from the beginning of the discharge at 20 mA cm^{-2}, roughly corresponding to the value attainable at 10 Hz by impedance spectroscopy.

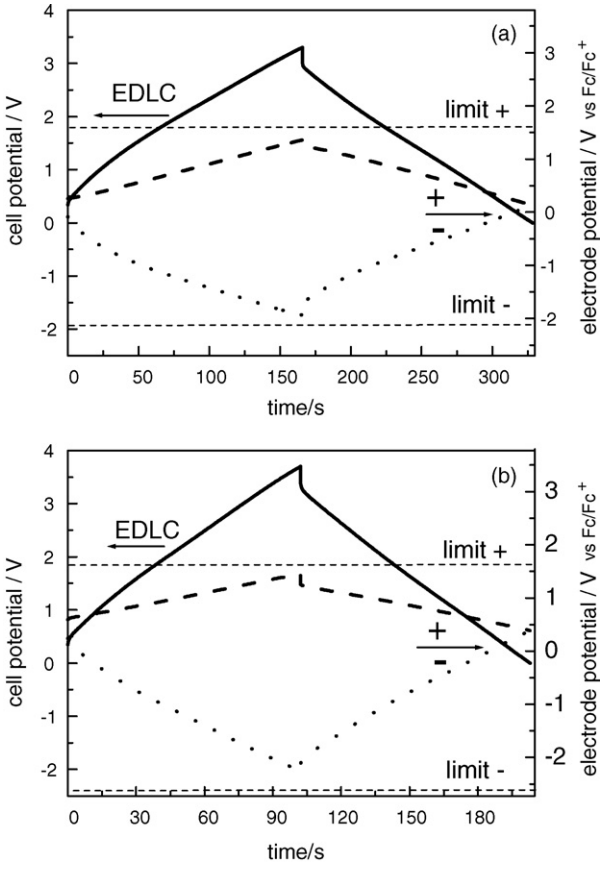

Fig. 5. Voltage profiles at 10 mA cm^{-2} and 60 °C of the (a) X3a/EMITFSI/X3a (5600th cycle, V_{max} = 3.3 V) and (b) X3a/$PYR_{14}TFSI$/X3a (15,300th cycle, V_{max} = 3.7 V) asymmetric EDLCs and of their positive and negative electrodes; dashed lines indicate maximum electrode potential excursions permitted by the two ILs.

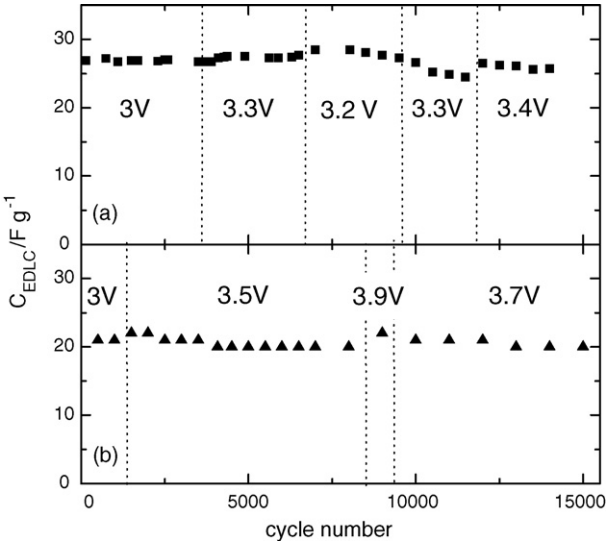

Fig. 6. Trend of supercapacitor specific capacitance (C_{EDLC}, in F per gram of total composite electrode materials) over cycling at 60 °C and 20 mA cm^{-2} of the (a) X3a/EMITFSI/X3a and (b) X3a/$PYR_{14}TFSI$/X3a asymmetric EDLCs with the indications of maximum cell voltages reached upon cycling.

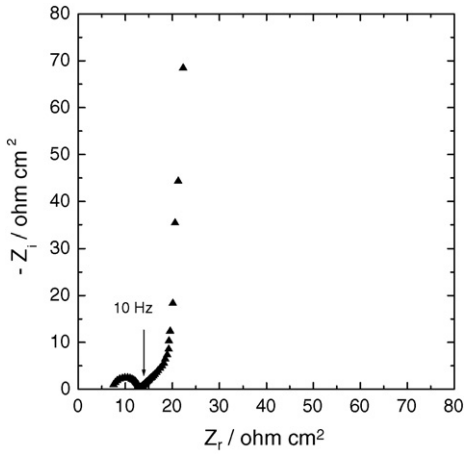

Fig. 7. Nyquist plot of the discharged X3a/PYR_{14}TFSI/X3a asymmetric EDLC at 60 °C (5×10^4 to 10^{-2} Hz frequency range).

The X3a/PYR_{14}TFSI/X3a EDLC displays a higher ESR than X3a/EMITFSI/X3a, mainly because of the ion conductivity of PYR_{14}TFSI, which is 6 mS cm^{-1} at 60 °C and lower than that of EMITFSI (25 mS cm^{-1} at the same temperature). However, the higher V_{max} of the former EDLC also ensures a higher P_{max} of 11.4 kW kg^{-1}. Note that the ESR in Table 3 is markedly affected by cell assembly. Indeed, the asymmetric EDLCs featured a very thick, 200 μm separator, which significantly contributes to ESR. This can be seen in the Nyquist plot of the X3a/PYR_{14}TFSI/X3a EDLC reported as an example in Fig. 7, where the impedance value at the highest frequency arising from electronic and ionic resistances is 7 Ω cm^2. A reduction of the ionic is feasible by using a 10-fold thinner separator, which does not limit the capacitance of the carbon electrodes because the high porosity of the X3a carbon provides an IL-reservoir for double-layer formation. On the other hand, we used home-made electrodes and it is well known that automatic lamination procedures help to decrease electrode contact resistances, which are mainly responsible for the resistive component of the high-frequency semicircle in the impedance spectrum in Fig. 7. Thus, the P_{max} values reported in Table 3 are to be taken as underestimated. The fast charge–discharge response of the X3a/PYR_{14}TFSI/X3a and X3a/EMITFSI/X3a EDLCs at 60° C is clearly evinced by the trends of their capacitance versus frequency reported in Fig. 8; in these plots the capacitance was calculated from the imaginary component of the impedance at each frequency and normalized for the different EDLCs to the corresponding limit capacitance at 10 mHz. Indeed, the double-layer charging process begins for both the EDLCs at 10 Hz and the capacitance reaches the limit value at ca. 10^{-1} Hz, which means that the maximum storage/delivery capability can be reached in ca. 10 s.

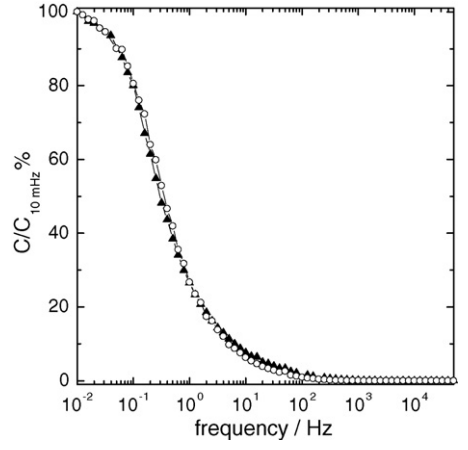

Fig. 8. Trends of the capacitance normalized to the limit value at 10 mHz (C/C_{10mHz}, %) vs. frequency of the (circle) X3a/EMITFSI/X3a and (triangle) X3a/PYR_{14}TFSI/X3a asymmetric EDLCs from impedance measurements at 60 °C.

4. Conclusions

CO_2 activation and heat treatment in Ar atmosphere of home-made xerogel carbons produced a mesoporous carbon featuring specific hydrophobic surface area $S_{>1.5nm}$ of 600 m^2 g^{-1} mainly from 15 nm pores and able to deliver more than 100 F g^{-1} in both EMITFSI and PYR_{14}TFSI ILs. We then developed asymmetric EDLCs with carbon loading at the positive electrode higher than that at the negative that makes it possible to charge each electrode up to the limit potentials defined by the ESW of each IL. Both EDLCs delivered over several thousands cycles at 60 °C a maximum specific energy of ca. 30 Wh kg^{-1} with V_{max} up to 3.4 V in the case of the X3a/EMITFSI/X3a and V_{max} of 3.7 V in the case of X3a/PYR_{14}TFSI/X3a, thereby outperforming commercial supercapacitors. Note that while 3.4 V is also attainable with a symmetric configuration, the V_{max} value of 3.7 V is achievable only by an asymmetric EDLC and, in the case of supercapacitors based on PYR_{14}TFSI, it represents a very safe value for long supercapacitor cycle life.

Acknowledgements

Work funded by the European Commission in the Sixth Framework Programme, Sub-programme Sustainable Surface Transport, under Contract No. TST4-CT-2005-518307 (Project ILHYPOS “Ionic Liquid-based Hybrid Supercapacitor”); all the partners in the Project are acknowledged.

References

[1] A. Burke, Electrochim. Acta 53 (2007) 1083–1091.
[2] A.G. Pandolfo, A.F. Hollenkamp, J. Power Sources 157 (2006) 11–27.
[3] J.R. Miller, Electrochim. Acta 52 (2006) 1703–1708.
[4] R. Kötz, M. Hahn, R. Gallay, J. Power Sources 154 (2006) 550–555.
[5] M. Galiński, A. Lewandowski, I. Stępniak, Electrochim. Acta 51 (2006) 5567–5580.
[6] A. Lewandowski, M. Galinski, J. Phys. Chem. Solids 65 (2004) 281–286.
[7] A. Balducci, W.A. Henderson, M. Mastragostino, S. Passerini, P. Simon, F. Soavi, Electrochim. Acta 50 (2005) 2233–2237.

[8] A. Balducci, R. Dugas, P.L. Taberna, P. Simon, D. Plée, M. Mastragostino, S. Passerini, J. Power Sources 165 (2007) 922–927.
[9] M. Lazzari, M. Mastragostino, F. Soavi, Electrochem. Commun. 9 (2007) 1567–1572.
[10] C. Arbizzani, S. Beninati, M. Lazzari, F. Soavi, M. Mastragostino, J. Power Sources 174 (2007) 648–652.
[11] M. Mastragostino, F. Soavi, J. Power Sources 174 (2007) 89–93.
[12] H.P. Bohem, Carbon 32 (1994) 759–769.
[13] A. Dandekar, R.T.K. Baker, M.A. Vannice, Carbon 36 (1998) 1821–1831.
[14] J.L. Figueiredo, M.F.R. Pereira, M.M.A. Freitas, J.J.M. Órfão, Carbon 37 (1999) 1379–1389.